Synergistic Toughening of Graphene Oxide–Molybdenum Disulfide–Thermoplastic Polyurethane Ternary Artificial Nacre

Sijie Wan,[†,§] Yuchen Li,[‡,§] Jingsong Peng,[†] Han Hu,[†] Qunfeng Cheng,[*,†] and Lei Jiang[†]

[†]Key Laboratory of Bio-inspired Smart Interfacial Science and Technology of Ministry of Education, School of Chemistry and Environment, BeiHang University, Beijing 100191, People's Republic of China and [‡]Beijing Engineering Research Center of Printed Electronics, Beijing Institute of Graphic Communication, Beijing 102600, People's Republic of China. [§]S. Wan and Y. Li contributed equally to the work.

ABSTRACT Inspired by the ternary structure of natural nacre, robust ternary artificial nacre is constructed through synergistic toughening of graphene oxide (GO) and molybdenum disulfide (MoS_2) nanosheets *via* a vacuum-assisted filtration self-assembly process. The synergistic toughening effect from high mechanical properties of GO and lubrication of MoS_2 nanosheets is successfully demonstrated. Meanwhile, the artificial nacre shows high electrical conductivity. This approach for constructing robust artificial nacre by synergistic effect from GO and MoS_2 provides a creative opportunity for designing and fabricating integrated artificial nacre in the near future, and this kind of ternary artificial nacre has great potential applications in aerospace, flexible supercapacitor electrodes, artificial muscle, and tissue engineering.

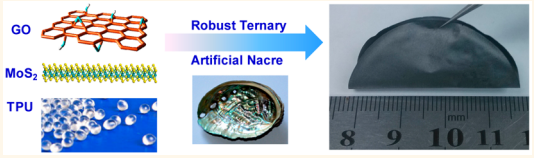

KEYWORDS: synergistic toughening · graphene oxide · molybdenum disulfide · ternary artificial nacre · mechanical properties

Natural nacre, consisting of two-dimensional (2D) aragonite platelets, one-dimensional (1D) nanofibrillar chitin, and protein, is a typical ternary structure.[1−5] Numerous reports describe nacre-inspired materials[6−9] that have achieved outstanding mechanical properties through constructing binary composites with various 2D inorganic building blocks, including man-made $CaCO_3$ platelets,[10,11] Al_2O_3 flakes,[12−14] layered double hydroxides,[15] nanoclay,[16−19] flattened double-walled carbon nanotubes,[20] and graphene oxide nanosheets.[21] However, it is common that the optimization of the tensile strength is at the expense of toughness,[22] namely, that it is difficult to simultaneously improve tensile strength and toughness of the binary nanocomposites due to relatively low stress-transfer efficiency. Recently, the synergistic effect from two fillers in the polymer matrix was developed[23] and demonstrated, for example, the ultratough rGO-CNT-PVA fiber.[24] We have demonstrated a robust ternary artificial nacre through synergistic toughening of nanoclay, nanofibrillar cellulose, and poly(vinyl alcohol).[25] The effective synergistic toughening in the ternary artificial nacre achieves high mechanical properties, superior to natural nacre and other binary layered nanoclay/polymer nanocomposites.

Herein, inspired by the synergistic action of building blocks in the ternary natural nacre, we have fabricated a robust ternary artificial nacre based on graphene oxide (GO)–molybdenum disulfide (MoS_2)–thermoplastic polyurethane (TPU) through vacuum-assisted filtration self-assembly. The synergistic toughening effect from the strengthening of GO and lubrication action of MoS_2 has been successfully revealed and demonstrated by optimizing the ratio of GO to MoS_2 in the ternary artificial nacre. The tensile strength and toughness are simultaneously improved and reach 1.7 and 3.8 times higher than that of natural nacre and superior to other commonly binary layered GO-based nanocomposites. Meanwhile, this kind of ternary artificial nacre shows high electrical conductivity. This novel principle for constructing robust artificial nacre by the synergistic effect from GO and MoS_2 opens new opportunities in the near future for designing and fabricating high-performance

* Address correspondence to cheng@buaa.edu.cn.

Received for review October 28, 2014 and accepted January 5, 2015.

Published online January 05, 2015
10.1021/nn506148w

© 2015 American Chemical Society

artificial nacre, and this kind of integrated ternary artificial nacre has great potential applications in aerospace, flexible supercapacitor electrodes, artificial muscle, and tissue engineering.

RESULTS AND DISCUSSION

The 2D MoS_2 nanosheet, an analogue of graphene,[26−29] has also drawn much attention due to its outstanding physical properties, such as catalytic, photovoltaic, lubricant, and mechanical properties.[27] A monolayer of MoS_2 has an extremely high breaking tensile strength (~23 GPa) and Young's modulus (~270 GPa)[30] and a high tensile strain (6−11%) compared to those of chemically reduced graphene, and it also has been used as the reinforcing building block for polymer composites. Therefore, MoS_2 is an ideal 2D nanosheet structure to construct the robust ternary artificial nacre with GO nanosheets. MoS_2 nanosheets were substantially and directly exfoliated from commercial MoS_2 powders using sonication.[26] Atomic force microscopy (AFM) images (Figure S1a) show that the size of GO is in the range 0.2−1 μm, and the thickness is about 0.75 nm. The size of exfoliated MoS_2 nanosheets (Figure S1b) is in the range 50−300 nm, and the thickness is about 1 nm, indicating monolayer MoS_2, which is consistent with the previous report.[26] Furthermore, the Raman spectra (Figure S1c) can confirm the exfoliated monolayer MoS_2 nanosheet. The two characteristic peaks of the monolayer MoS_2 nanosheet of in-plane E_{2g}^1 and out-of-plane A_{1g} vibration modes are at 384 and 403 cm^{-1}, respectively, and the distance between them is 19 cm^{-1}, which is in excellent agreement with the characteristics of monolayer MoS_2 as previous report.[31] On the other hand, the presence of the E_{2g}^1 Raman mode proves the exfoliated MoS_2 monolayer is 2H-MoS_2 not 1T-MoS_2.[32] Moreover, the Raman spectra in the broadened range of 100−700 cm^{-1} shows absent low-frequency regime peaks at 156 cm^{-1} (J_1), 226 cm^{-1} (J_2), and 333 cm^{-1} (J_3) of 1T-MoS_2,[32] which further confirms the exfoliated MoS_2 monolayer is the 2H polytype. Thus, the monolayer MoS_2 nanosheets with 2H polytype are successfully exfoliated in this study.

Before fabricating the ternary GO-MoS_2-TPU artificial nacre, the binary GO−TPU nanocomposites were assembled through vacuum-assisted filtration to optimize the ratio of GO to TPU in the nanocomposites. Three different weight ratios of GO to TPU (50:50, 70:30, 90:10) were selected. SEM images show a typical nacre-like layered structure, and with GO content increasing, the layered structure is clear, as shown in Figure S2. The X-ray diffraction (XRD) results indicate that the interlayer distance (*d*-spacing) increases from 8.31 Å ($2\theta = 10.64°$) for pure GO film to 8.58 Å ($2\theta = 10.30°$) for GO-TPU (90:10), as shown in Figure S3a and Table S2. The improvement of *d*-spacing shows the successful addition of TPU molecules into the GO galleries. The typical stress−strain curves of binary GO-TPU nanocomposites are shown in Figure S4. Previous reports have demonstrated that the tensile strength of GO-reinforced TPU nanocomposites increases with increasing GO content (<50 wt %),[33−35] and the strain dramatically drops when increasing the GO content, resulting in low toughness. In this study, it is obvious that the tensile strength and toughness of binary GO-TPU increase with GO content. Thus, the initial inorganic content was determined to be 90 wt % for constructing the GO-MoS_2-TPU ternary artificial nacre in the following experiments.

The fabrication process of the ternary artificial nacre is shown in Figure 1a. Four kinds of ternary GO-MoS_2-TPU artificial nacre (Figure 1b) with 10 wt % TPU were prepared: GO-MoS_2-TPU-I (GO:MoS_2 = 97.5:2.5), GO-MoS_2-TPU-II (GO:MoS_2 = 95:5), GO-MoS_2-TPU-III (GO:MoS_2 = 90:10), and GO-MoS_2-TPU-IV (GO:MoS_2 = 80:20), respectively. The real mass percentages of MoS_2 and GO were confirmed by thermogravimetric analysis (TGA), as shown in Figure S5 and Table S1. The cross-section morphology of ternary rGO-MoS_2-TPU-II is a typical layered structure (Figure 1c). The energy-dispersive X-ray spectroscopy (EDS) was performed on this cross-section, and the result of EDS shows a uniform distribution of element Mo in Figure 1d, indicating that the MoS_2 nanosheets were uniformly dispersed in the GO interlayers. The cross-section morphology and EDS of other ternary rGO-MoS_2-TPU artificial nacres also indicate the uniform distribution of Mo element, as shown in Figure S6. In addition, XRD results further confirm the well-ordered intercalation of MoS_2 into the GO interlayers. The *d*-spacing of ternary GO-MoS_2-TPU nanocomposites is listed in Table S2. With increasing MoS_2 content, the *d*-spacing increases from 8.71 Å for GO-MoS_2-TPU-I to 10.39 Å for GO-MoS_2-TPU-IV. Moreover, for the ternary GO-MoS_2-TPU nanocomposites, the distinct peak at approximately 14° (2θ), associated with 002 reflection from the basal plane of MoS_2 (Figure S3), suggests that MoS_2 nanosheets tend to restack during the process of vacuum-assisted filtration,[26] which was also confirmed by the cross-section TEM image of rGO-MoS_2-TPU-II, as shown in Figure S7.

The comparison stress−strain curves of pure GO, binary GO-TPU (90:10) nanocomposite, and ternary GO-MoS_2-TPU-II artificial nacre are shown in Figure 2a, and the detailed mechanical properties of binary and ternary artificial nacre are listed in Table S3. It is obvious that the ternary GO-MoS_2-TPU artificial nacre shows an excellent integration of tensile strength and toughness, much higher than the binary GO-TPU nanocomposites. For example, the tensile strength and toughness of rGO-MoS_2-TPU-II reach 235.3 ± 19.4 MPa and 6.9 ± 0.5 $MJ \cdot m^{-3}$, respectively, which are 40% and 100% higher than rGO-TPU (90:10), with a tensile strength of 166.7 ± 9.7 MPa and toughness of 3.3 ± 0.3 $MJ \cdot m^{-3}$.

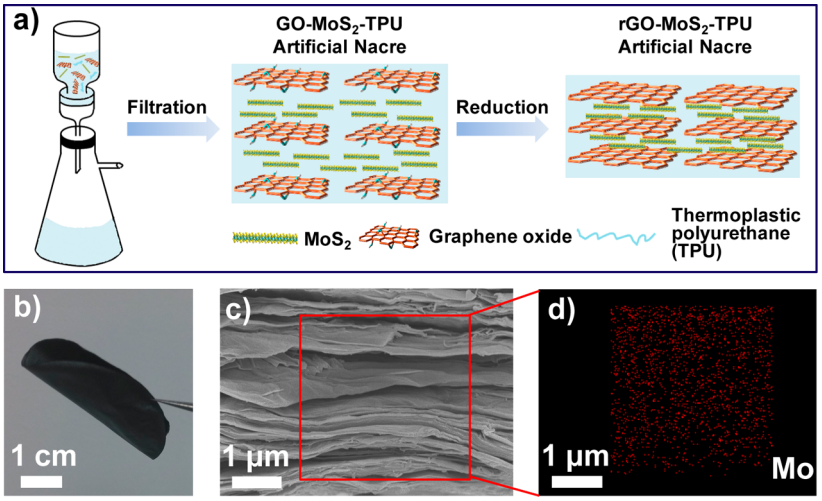

Figure 1. Illustration of the preparation process of the ternary artificial nacre of GO-MoS_2-TPU through vacuum-assisted filtration self-assembly. (a) The GO nanosheets were dispersed into dimethylformamide (DMF) by stirring and sonication. Then TPU/DMF solution and MoS_2/NMP solution was added into the GO solution. After sonication, the uniform suspension was vacuum-assisted filtrated into the ternary artificial nacre. (b) Digital image of ternary rGO-MoS_2-TPU artificial nacre. (c) SEM image of the cross-section of rGO-MoS_2-TPU-II. (d) Corresponding EDS of Mo element originating from MoS_2 in rGO-MoS_2-TPU-II, revealing that MoS_2 nanosheets are homogeneously distributed without aggregation.

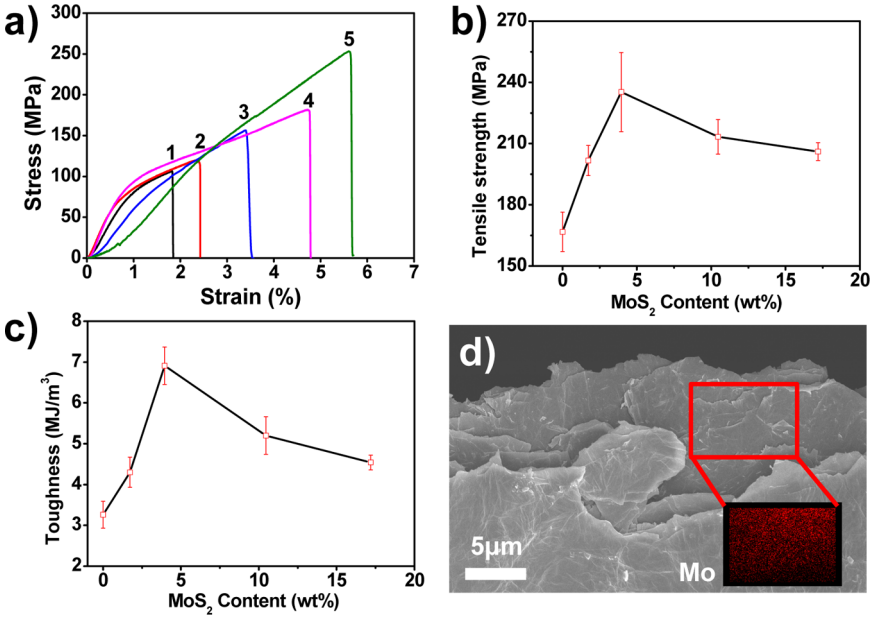

Figure 2. (a) Tensile stress−strain curves of GO film (curve 1), binary GO-TPU (90:10) nanocomposite (curve 2), rGO-TPU nanocomposite (curve 3), ternary GO-MoS_2-TPU-II nanocomposites (curve 4), and ternary rGO-MoS_2-TPU-II nanocomposites (curve 5). (b and c) The tensile strength and toughness of nanocomposites with different MoS_2 contents, indicating that the tensile strength and toughness show a maximum value when the MoS_2 content is about 4.0 wt %. (d) Fracture morphology of ternary rGO-MoS_2-TPU-II nanocomposites. The inset is EDS of elemental Mo, indicating much more friction between rGO and MoS_2 nanosheets and the lubrication of MoS_2 occurred in the fracture process.

Compared to natural nacre (tensile strength of 80−135 MPa and toughness of 1.8 $MJ \cdot m^{-3}$),[36] the tensile strength and toughness of the ternary rGO-MoS_2-TPU-II artificial nacre are simultaneously improved to be 1.7 and 3.8 times higher. The corresponding fracture morphology of the ternary rGO-MoS_2-TPU-II artificial nacre is shown in Figure 2d. The rGO nanosheets are pulled out, and the MoS_2 was clearly observed on the surface of the rGO nanosheets (inset in Figure 2d), indicating that much more friction between rGO and MoS_2 nanosheets and the lubrication of MoS_2 occurred in the fracture process. Thus, the synergistic toughening from GO and MoS_2 nanosheets takes place in the ternary artificial nacre, which could absorb much more energy than the binary nanocomposites.

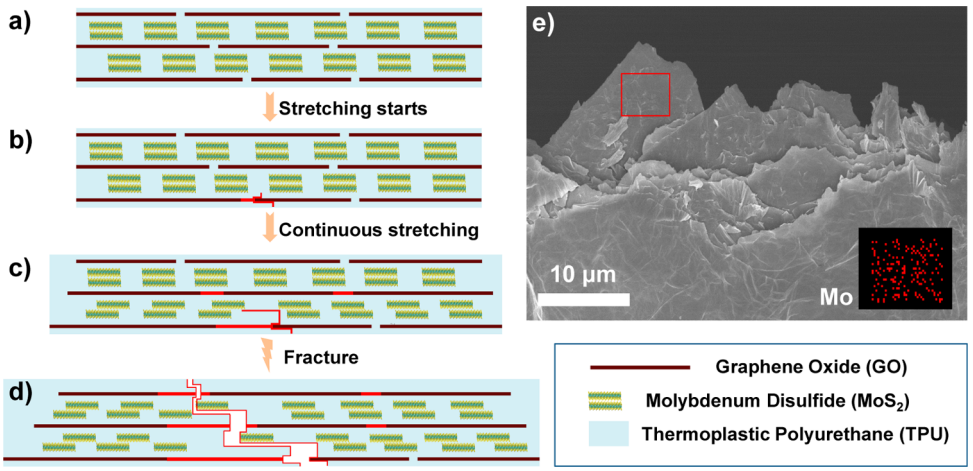

Figure 3. Proposed synergistic mechanism of ternary rGO-MoS_2-TPU artificial nacre. (a) When stretching starts, (b) the rGO nanosheets begin to slide and initiate the crack. (c) With continuous stretching, the MoS_2 nanosheets bridge the crack through lubrication and offer resistance to rGO nanosheet sliding, initiating the sliding sites of the adjacent rGO nanosheets. (d) Finally, the ternary rGO-MoS_2-TPU artificial nacre fractures under the mode of rGO and MoS_2 nanosheet pull-out. (e) The fracture morphology of ternary rGO-MoS_2-TPU artificial nacre shows that the GO nanosheets are pulled out. Mo element was observed on the surface of rGO nanosheets (inset image), indicating the lubrication from MoS_2 happened between rGO nanosheets.

What is the optimal ratio between GO and MoS_2 to achieve the maximum synergistic toughening effect? Four different ratios between GO and MoS_2 were selected in the fabrication of ternary artificial nacre, as described before. The MoS_2 content by TGA in the ternary GO-MoS_2-TPU-I, GO-MoS_2-TPU-II, GO-MoS_2-TPU-III, and GO-MoS_2-TPU-IV artificial nacre, is 1.7, 4.0, 10.5, and 17.2 wt % (Figure S5), respectively. As shown in Figure 2b and c, with MoS_2 content increasing from 1.7 wt % to 4.0 wt %, the tensile strength and toughness reach a maximum. Further additions of MoS_2 nanosheets decrease the tensile strength and toughness, revealing that more MoS_2 damages the synergistic toughening effect.

To explore the synergistic toughening effect from GO and MoS_2, a crack extension model is proposed, as shown in Figure 3. When initially subjected to stress, the hydrogen bonds between rGO nanosheets and TPU are broken due to fracture, and the rGO nanosheets begin to slide over each other, leading to the formation of cracks (Figure 3b). Subsequently, the friction between MoS_2 and GO nanosheets, triggers the movement of the MoS_2 nanosheets along the rGO nanosheets. The sliding between molybdenum and sulfur nanolayers easily occurs due to the lubrication action from the 2H MoS_2, which means that the propagating crack would be deflected by MoS_2 nanosheets (Figure 3c). Thus, much energy is being absorbed in this procedure. When continuously stretching, the layered nanostructure of restacked MoS_2 separates into a few layers of MoS_2 nanosheets. The crack would further propagate along the adjacent rGO nanosheets and be deflected by MoS_2 nanosheets. This cycling of crack initiation−propagation−deflection would continue until the ternary rGO-MoS_2-TPU artificial nacre fractures (Figure 3d), resulting in more energy dissipation and large strain. The rGO nanosheets were pulled out and the layered structure of MoS_2 was damaged; the corresponding fracture morphology is shown in Figure 3e. All ternary artificial nacres have similar fracture morphology, including front and side views, as shown in Figure S8. Mo element was observed on the surface of rGO nanosheets, indicating the lubrication from MoS_2 happened between rGO nanosheets. This kind of synergistic mode of rGO pull-out and sliding of the layered structure of MoS_2 is superior to our previously proposed synergistic mode of 2D MMT platelet and 1D nanofibril pull-out.[25] Thus, the energy dissipation of the ternary rGO-MoS_2-TPU artificial nacre is much higher, resulting in an integrated high tensile strength and toughness.

Although the lubrication of MoS_2 plays a key role in the synergistic toughening, the critical amount of MoS_2 is optimized to be about 4.0 wt % in the ternary artificial nacre. Below 4.0 wt %, the crack could not be effectively deflected by MoS_2 nanosheets and the energy dissipation through slippage of MoS_2 nanosheets would be low, resulting in less improvement in tensile strength and toughness. On the other hand, if the content of MoS_2 is higher than 4.0 wt %, the MoS_2 would form excessive restacking, which has been confirmed by the XRD results (Figure S3), leading to the low efficiency of stress transfer from MoS_2 nanosheets to adjacent rGO nanosheets and low energy dissipation. The tensile strength and toughness of the ternary artificial nacre still cannot be dramatically improved.

The advantages of this ternary artificial nacre are the integrated strength and toughness compared with

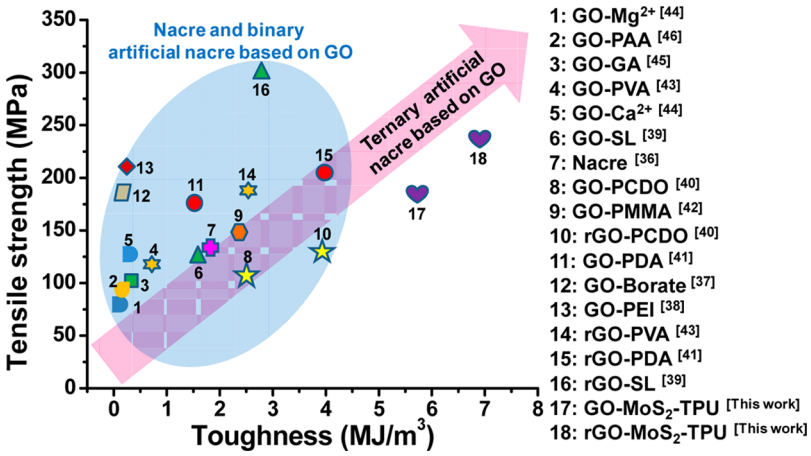

Figure 4. Comparison of tensile strength and toughness of our ternary artificial nacre, other binary layered GO-based materials, and natural nacre. The ternary rGO-MoS_2-TPU-II artificial nacre shows strong integrated strength and toughness compared with other binary layered materials based on GO (the inset blue oval), such as hydrogen interaction of GO-PVA[43] and GO-SL,[39] ionic interaction of GO-Ca^{2+} [44] and GO-Mg^{2+},[44] short-chain covalent cross-linking of GO-GA[45] and PGO-PEI,[38] and long-chain covalent cross-linking of GO-PCDO[40] and GO-PDA.[41]

natural nacre and other binary nacre-like materials based on GO nanosheets (Figure 4). The GO-based binary nacre-like materials (the inset blue oval) show improvement in only one mechanical property, such as tensile strength or stiffness or toughness, as evidenced, for example, in highly stiff bioinspired GO-layered materials through borate cross-linking (GO-Borate).[37] The stiffness is as high as 127 ± 4 GPa. However, the strain of GO-Borate materials is only 0.15%, and the toughness is as low as 0.14 $MJ \cdot m^{-3}$, lower than one-tenth of natural nacre.[36] High tensile strength nacre-like materials through poly(ether imide) (PEI) cross-linking GO sheets (PGO-PEI) have been realized recently.[38] The tensile strength reaches 209.9 MPa; however the elongation is only 0.22% and the toughness is only 0.23 $MJ \cdot m^{-3}$, which is still only one-eighth of natural nacre.[36] Although, the high tensile strength rGO-based materials with 300 MPa at low silk fibroin content (2.5%) (rGO-SL) has been demonstrated.[39] However, the toughness is only 2.8 $MJ \cdot m^{-3}$, which is lower than our previous reports (rGO-PCDO of 3.91 $MJ \cdot m^{-3}$ [40] and rGO-PDA of 4.0 $MJ \cdot m^{-3}$ [41]).

The tensile strength of rGO-MoS_2-TPU-II artificial nacre is comparable to rGO-SL[39] and higher than GO-PEI.[38] The toughness of rGO-MoS_2-TPU-II is 1.5-fold and 29-fold higher than rGO-SL and GO-PEI, respectively. This novel strategy to fabricate ternary GO-based nanocomposites is also superior to other approaches for constructing binary GO-based layered materials, such as hydrogen interaction between GO nanosheets and a matrix (*e.g.*, GO-PMMA,[42] rGO-PVA,[43]), ion interaction between GO nanosheets and a matrix (*e.g.*, GO-Mg^{2+},[44] GO-Ca^{2+},[44]), and other covalent bonding, including glutaraldehyde (GA) covalent cross-linking (GO-GA)[45] and polyallylamine (PAA) cross-linking (GO-PAA).[46] The detailed mechanical properties of our artificial nacre, natural nacre, and other GO-based layered materials are listed in Table S4. It should be noted that while this novel technique successfully demonstrated the fabrication of high-performance ternary artificial nacre, it still needs to be further refined by scaling for mass production. The fantastic structure of natural nacre inspires us to construct integrated high tensile strength and toughness artificial nacre, which is a research goal shared by many groups working on bioinspired layered materials. The pink arrow in Figure 4 illustrates the trend in integrated high performance, driving the future of bioinspired layered materials.

Although electrical conductivity of the ternary rGO-MoS_2-TPU artificial nacre shows a small decrease when adding the semiconductor MoS_2 (Table S1), the electrical conductivity of rGO-MoS_2-TPU-IV artificial nacre is still as high as 46.4 $S \cdot cm^{-1}$, which is higher than that of rGO-PDA[41] and comparable to that of the pure rGO film.[47] The rGO-MoS_2-TPU-II artificial nacre as the conducting wire is demonstrated in a circuit, as shown in Figure S9. Furthermore, a blue LED could be steadily lighted when strongly bending the ternary artificial nacre (Movie S1), indicating the potential application in flexible devices.

CONCLUSION

In conclusion, inspired by the ternary natural nacre, we successfully fabricated robust ternary artificial nacre through synergistic toughening of graphene oxide and molybdenum disulfide nanosheets *via* a vacuum-assisted filtration self-assembly process. The synergistic toughening effect from high mechanical properties of GO and lubrication of MoS_2 nanosheets is successfully demonstrated. In addition, the artificial nacre shows high electrical conductivity. This study opens the door toward constructing robust artificial nacre by synergistic toughening in the near future.

This kind of integrated ternary artificial nacre with excellent toughness shows great promise for applications in aerospace, flexible supercapacitor electrodes, artificial muscles, and tissue engineering.

METHODS

Materials. Graphene oxide sheets were purchased from XianFeng NANO Co., Ltd. MoS_2 powders, 57 wt % hydroiodic acid (HI), and 1-methyl-2-pyrrolidinone (NMP, anhydrous, 99.5%) were purchased from Sigma-Aldrich. Thermoplastic polyurethane was purchased from BASF Corp. MoS_2 nanosheets were exfoliated from MoS_2 powders by liquid exfoliation according to the previous report.[26] More detailed exfoliation procedures are as follow: the MoS_2 powders were added to NMP with an initial concentration of 6 mg/mL. After sonication for 3 h, the dispersion was settled for 12 h. Then the dispersion was centrifuged at 2000 rpm for 30 min. Subsequently, the top 3/4 of the dispersion was collected as the exfoliated MoS_2 nanosheet dispersion for the following experiments.

Fabrication of Ternary GO-MoS2-TPU Artificial Nacre. The obtained as-prepared MoS_2 dispersion and TPU solution was successively added to the GO solution at different ratios. The mixtures were stirred and sonicated for 3 and 1 h, respectively, to form a homogeneous solution. With vacuum-assisted filtration, the homogeneous solution was assembled to the ternary artificial nacre. Finally, the dried ternary artificial nacre was reduced through immersing into the HI solution. The oxidized iodine on the surface of rGO-MoS_2-TPU artificial nacre was cleaned off with ethanol washing for 4 days.

Characterization. Scanning electron microscopy (SEM) images were obtained by a field-emission scanning electron microscope (JEOL-7500F). The atomic force microscopy was characterized by a Leica TCS SP5. TEM images were obtained using a FEI Tecnai G20 instrument at 200 kV. Thermogravimetric analysis was done using a TG/DTA6300 NSK under air with a temperature increase of 10 °C/min. Raman spectroscopy measurements was performed on a LabRAM HR800 (Horiba Jobin Yvon) with an excitation energy of 1.96 eV (633 nm). X-ray diffraction profiles were carried out with Cu Kα radiation (λ = 1.54 nm). The mechanical properties were measured in the tensile mode using a Shimadzu AGS-X tester at a loading rate of 1 mm/min with a gauge length of 5 mm. All of the samples were cut into strips with a length of 20 mm and a width of 3 mm before measuring. The results for each sample are based on the average value of 3−5 specimens. The electrical conductivities of the ternary artificial nacre were measured by a standard two-probe method using a source meter (Agilent E4980A).

Conflict of Interest: The authors declare no competing financial interest.

Acknowledgment. This work was supported by the National Natural Science Foundation of China (21273017, 51103004), the National Research Fund for Fundamental Key Projects (2010CB934700), Program for New Century Excellent Talents in University (NCET-12-0034), Beijing Nova Program (Z121103002512020), Beijing Science and Technology Program (Z121100001312004), Fok Ying-Tong Education Foundation (141045), Open Project of Beijing National Laboratory for Molecular Sciences and the 111 Project (B14009), and the Fundamental Research Funds for the Central Universities (YWF-14-HXXY-018). We thank Prof. Zhou Li (BeiHang University) for his help in electrical conductivity testing.

Supporting Information Available: This material is available free of charge *via* the Internet at http://pubs.acs.org.

REFERENCES AND NOTES

1. Weiner, S.; Traub, W.; Parker, S. B. Macromolecules in Mollusc Shells and Their Functions in Biomineralization [and Discussion]. *Philos. Trans. R. Soc., B* **1984**, *304*, 425–434.
2. Levi-Kalisman, Y.; Falini, G.; Addadi, L.; Weiner, S. Structure of the Nacreous Organic Matrix of a Bivalve Mollusk Shell Examined in the Hydrated State Using Cryo-TEM. *J. Struct. Biol.* **2001**, *135*, 8–17.
3. Nudelman, F.; Chen, H. H.; Goldberg, H. A.; Weiner, S.; Addadi, L. Spiers Memorial Lecture Lessons from Biomineralization: Comparing the Growth Strategies of Mollusc Shell Prismatic and Nacreous Layers in Atrina Rigida. *Faraday Discuss.* **2007**, *136*, 9–25.
4. Meyers, M. A.; Chen, P. Y.; Lin, A. Y. M.; Seki, Y. Biological Materials: Structure and Mechanical Properties. *Prog. Mater. Sci.* **2008**, *53*, 1–206.
5. Lin, A. Y.-M.; Meyers, M. A. Interfacial Shear Strength in Abalone Nacre. *J. Mech. Behav. Biomed. Mater.* **2009**, *2*, 607–612.
6. Espinosa, H. D.; Rim, J. E.; Barthelat, F.; Buehler, M. J. Merger of Structure and Material in Nacre and Bone-Perspectives on de Novo Biomimetic Materials. *Prog. Mater. Sci.* **2009**, *54*, 1059–1100.
7. Studart, A. R. Towards High-Performance Bioinspired Composites. *Adv. Mater.* **2012**, *24*, 5024–5044.
8. Meyers, M. A.; McKittrick, J.; Chen, P.-Y. Structural Biological Materials: Critical Mechanics-Materials Connections. *Science* **2013**, *339*, 773–779.
9. Yao, H.-B.; Ge, J.; Mao, L.-B.; Yan, Y.-X.; Yu, S.-H. 25th Anniversary Article: Artificial Carbonate Nanocrystals and Layered Structural Nanocomposites Inspired by Nacre: Synthesis, Fabrication and Applications. *Adv. Mater.* **2014**, *26*, 163–188.
10. Finnemore, A.; Cunha, P.; Shean, T.; Vignolini, S.; Guldin, S.; Oyen, M.; Steiner, U. Biomimetic Layer-by-Layer Assembly of Artificial Nacre. *Nat. Commun.* **2012**, *3*, 966.
11. Li, X. Q.; Zeng, H. C. Calcium Carbonate Nanotablets: Bridging Artificial to Natural Nacre. *Adv. Mater.* **2012**, *24*, 6277–6282.
12. Deville, S.; Saiz, E.; Nalla, R. K.; Tomsia, A. P. Freezing as a Path to Build Complex Composites. *Science* **2006**, *311*, 515–518.
13. Bonderer, L. J.; Studart, A. R.; Gauckler, L. J. Bioinspired Design and Assembly of Platelet Reinforced Polymer Films. *Science* **2008**, *319*, 1069–1073.
14. Bouville, F.; Maire, E.; Meille, S.; Van de Moortele, B.; Stevenson, A. J.; Deville, S. Strong, Tough and Stiff Bioinspired Ceramics from Brittle Constituents. *Nat. Mater.* **2014**, *13*, 508–514.
15. Yao, H.-B.; Fang, H.-Y.; Tan, Z.-H.; Wu, L.-H.; Yu, S.-H. Biologically Inspired, Strong, Transparent, and Functional Layered Organic−Inorganic Hybrid Films. *Angew. Chem., Int. Ed.* **2010**, *49*, 2140–2145.
16. Tang, Z.; Kotov, N. A.; Magonov, S.; Ozturk, B. Nanostructured Artificial Nacre. *Nat. Mater.* **2003**, *2*, 413–418.
17. Podsiadlo, P.; Kaushik, A. K.; Arruda, E. M.; Waas, A. M.; Shim, B. S.; Xu, J. D.; Nandivada, H.; Pumplin, B. G.; Lahann, J.; Ramamoorthy, A.; *et al.* Ultrastrong and Stiff Layered Polymer Nanocomposites. *Science* **2007**, *318*, 80–83.
18. Walther, A.; Bjurhager, I.; Malho, J.-M.; Pere, J.; Ruokolainen, J.; Berglund, L. A.; Ikkala, O. Large-Area, Lightweight and Thick Biomimetic Composites with Superior Material Properties *via* Fast, Economic, and Green Pathways. *Nano Lett.* **2010**, *10*, 2742–2748.
19. Walther, A.; Bjurhager, I.; Malho, J.-M.; Ruokolainen, J.; Berglund, L.; Ikkala, O. Supramolecular Control of Stiffness and Strength in Lightweight High-Performance Nacre-Mimetic Paper with Fire-Shielding Properties. *Angew. Chem., Int. Ed.* **2010**, *49*, 6448–6453.
20. Cheng, Q.; Li, M.; Jiang, L.; Tang, Z. Bioinspired Layered Composites Based on Flattened Double-Walled Carbon Nanotubes. *Adv. Mater.* **2012**, *24*, 1838–1843.

21. Cheng, Q.; Jiang, L.; Tang, Z. Bioinspired Layered Materials with Superior Mechanical Performance. *Acc. Chem. Res.* **2014**, *47*, 1256–1266.
22. Ritchie, R. O. The Conflicts between Strength and Toughness. *Nat. Mater.* **2011**, *10*, 817–822.
23. Prasad, K. E.; Das, B.; Maitra, U.; Ramamurty, U.; Rao, C. N. R. Extraordinary Synergy in the Mechanical Properties of Polymer Matrix Composites Reinforced with 2 Nanocarbons. *Proc. Natl. Acad. Sci. U.S.A.* **2009**, *106*, 13186–13189.
24. Shin, M. K.; Lee, B.; Kim, S. H.; Lee, J. A.; Spinks, G. M.; Gambhir, S.; Wallace, G. G.; Kozlov, M. E.; Baughman, R. H.; Kim, S. J. Synergistic Toughening of Composite Fibres by Self-Alignment of Reduced Graphene Oxide and Carbon Nanotubes. *Nat. Commun.* **2012**, *3*, 650.
25. Wang, J.; Cheng, Q.; Lin, L.; Jiang, L. Synergistic Toughening of Bioinspired Poly(vinyl alcohol)−Clay−Nanofibrillar Cellulose Artificial Nacre. *ACS Nano* **2014**, *8*, 2739–2745.
26. Coleman, J. N.; Lotya, M.; O'Neill, A.; Bergin, S. D.; King, P. J.; Khan, U.; Young, K.; Gaucher, A.; De, S.; Smith, R. J.; *et al.* Two-Dimensional Nanosheets Produced by Liquid Exfoliation of Layered Materials. *Science* **2011**, *331*, 568–571.
27. Huang, X.; Zeng, Z. Y.; Zhang, H. Metal Dichalcogenide Nanosheets: Preparation, Properties and Applications. *Chem. Soc. Rev.* **2013**, *42*, 1934–1946.
28. Rao, C. N. R.; Ramakrishna Matte, H. S. S.; Maitra, U. Graphene Analogues of Inorganic Layered Materials. *Angew. Chem., Int. Ed.* **2013**, *52*, 13162–13185.
29. Rao, C. N. R.; Maitra, U.; Waghmare, U. V. Extraordinary Attributes of 2-Dimensional MoS_2 Nanosheets. *Chem. Phys. Lett.* **2014**, *609*, 172–183.
30. Bertolazzi, S.; Brivio, J.; Kis, A. Stretching and Breaking of Ultrathin MoS_2. *ACS Nano* **2011**, *5*, 9703–9709.
31. Lee, C.; Yan, H.; Brus, L. E.; Heinz, T. F.; Hone, J.; Ryu, S. Anomalous Lattice Vibrations of Single- and Few-Layer MoS_2. *ACS Nano* **2010**, *4*, 2695–2700.
32. Jiménez Sandoval, S.; Yang, D.; Frindt, R. I. J. Raman Study and Lattice Dynamics of Single Molecular Layers of MoS_2. *Phys. Rev. B* **1991**, *44*, 3955–3962.
33. Liang, J. J.; Xu, Y. F.; Huang, Y.; Zhang, L.; Wang, Y.; Ma, Y. F.; Li, F. F.; Guo, T. Y.; Chen, Y. S. Infrared-Triggered Actuators from Graphene-Based Nanocomposites. *J. Phys. Chem. C* **2009**, *113*, 9921–9927.
34. Nguyen, D. A.; Lee, Y. R.; Raghu, A. V.; Jeong, H. M.; Shin, C. M.; Kim, B. K. Morphological and Physical Properties of a Thermoplastic Polyurethane Reinforced with Functionalized Graphene Sheet. *Polym. Int.* **2009**, *58*, 412–417.
35. Wang, X.; Hu, Y. A.; Song, L.; Yang, H. Y.; Xing, W. Y.; Lu, H. D. *In Situ* Polymerization of Graphene Nanosheets and Polyurethane with Enhanced Mechanical and Thermal Properties. *J. Mater. Chem.* **2011**, *21*, 4222–4227.
36. Jackson, A.; Vincent, J.; Turner, R. The Mechanical Design of Nacre. *Proc. R. Soc., B* **1988**, *234*, 415–440.
37. An, Z.; Compton, O. C.; Putz, K. W.; Brinson, L. C.; Nguyen, S. T. Bio-Inspired Borate Cross-Linking in Ultra-Stiff Graphene Oxide Thin Films. *Adv. Mater.* **2011**, *23*, 3842–3846.
38. Tian, Y.; Cao, Y. W.; Wang, Y.; Yang, W. L.; Feng, J. C. Realizing Ultrahigh Modulus and High Strength of Macroscopic Graphene Oxide Papers through Crosslinking of Mussel-Inspired Polymers. *Adv. Mater.* **2013**, *25*, 2980–2983.
39. Hu, K. S.; Tolentino, L. S.; Kulkarni, D. D.; Ye, C. H.; Kumar, S.; Tsukruk, V. V. Written-in Conductive Patterns on Robust Graphene Oxide Biopaper by Electrochemical Microstamping. *Angew. Chem., Int. Ed.* **2013**, *52*, 13784–13788.
40. Cheng, Q. F.; Wu, M. X.; Li, M. Z.; Jiang, L.; Tang, Z. Y. Ultratough Artificial Nacre Based on Conjugated Cross-linked Graphene Oxide. *Angew. Chem., Int. Ed.* **2013**, *52*, 3750–3755.
41. Cui, W.; Li, M.; Liu, J.; Wang, B.; Zhang, C.; Jiang, L.; Cheng, Q. A Strong Integrated Strength and Toughness Artificial Nacre Based on Dopamine Cross-Linked Graphene Oxide. *ACS Nano* **2014**, *8*, 9511–9517.
42. Putz, K. W.; Compton, O. C.; Palmeri, M. J.; Nguyen, S. T.; Brinson, L. C. High-Nanofiller-Content Graphene Oxide−Polymer Nanocomposites *via* Vacuum-Assisted Self-Assembly. *Adv. Funct. Mater.* **2010**, *20*, 3322–3329.
43. Li, Y.-Q.; Yu, T.; Yang, T.-Y.; Zheng, L.-X.; Liao, K. Bio-Inspired Nacre-like Composite Films Based on Graphene with Superior Mechanical, Electrical, and Biocompatible Properties. *Adv. Mater.* **2012**, *24*, 3426–3431.
44. Park, S.; Lee, K. S.; Bozoklu, G.; Cai, W.; Nguyen, S. T.; Ruoff, R. S. Graphene Oxide Papers Modified by Divalent Ions - Enhancing Mechanical Properties *via* Chemical Cross-Linking. *ACS Nano* **2008**, *2*, 572–578.
45. Gao, Y.; Liu, L.-Q.; Zu, S.-Z.; Peng, K.; Zhou, D.; Han, B.-H.; Zhang, Z. The Effect of Interlayer Adhesion on the Mechanical Behaviors of Macroscopic Graphene Oxide Papers. *ACS Nano* **2011**, *5*, 2134–2141.
46. Park, S.; Dikin, D. A.; Nguyen, S. T.; Ruoff, R. S. Graphene Oxide Sheets Chemically Cross-Linked by Polyallylamine. *J. Phys. Chem. C* **2009**, *113*, 15801–15804.
47. Chen, H.; Müller, M. B.; Gilmore, K. J.; Wallace, G. G.; Li, D. Mechanically Strong, Electrically Conductive, and Biocompatible Graphene Paper. *Adv. Mater.* **2008**, *20*, 3557–3561.